J. Fluid Mech. (2014), *vol.* 757, *pp.* 208–230.
doi:10.1017/jfm.2014.407

Interaction of two axisymmetric bodies falling in tandem at moderate Reynolds numbers

Nicolas Brosse[1,2] **and Patricia Ern**[1,2,†]

[1]Université de Toulouse; INPT, UPS; IMFT (Institut de Mécanique des Fluides de Toulouse), Allée Camille Soula, F-31400 Toulouse, France

[2]CNRS; IMFT; F-31400 Toulouse, France

(Received 19 December 2013; revised 30 May 2014; accepted 13 July 2014; first published online 19 September 2014)

This study considers the interaction of two identical solid axisymmetric bodies (of diameter d and thickness h) freely falling in a fluid at rest. We determine the domains of existence of the different interaction behaviour of the two bodies (i.e. attraction, repulsion and indifference) as a function of their initial relative position. We then investigate in detail the case of bodies falling in tandem, for both rectilinear and periodic paths, and the associated attraction behaviour. For all the Reynolds numbers and aspect ratios of the bodies ($\chi = d/h$) investigated, the trailing body catches up with the leading body. We provide a quantitative description of the kinematics leading to the regrouping of the bodies and analyse its relationship with the wake of the leading body. In the case of rectilinear paths, a dynamical model that takes into account the axial evolution of the wake of the leading body is proposed to reproduce the acceleration observed for the trailing body until a vertical separation distance between the bodies of 1.5 diameters. In parallel, direct numerical simulations (DNS) of the flow about two fixed bodies in tandem in an oncoming flow are carried out, providing a good estimation of the motion of the bodies for separation distances larger than 5 diameters. For periodic paths, the kinematics leading to the regrouping of the bodies is slower than for rectilinear paths. However, in this case, the interaction also leads to significant changes in the characteristics of the oscillatory motion and is strongly dependent on the aspect ratio of the bodies. To explain the observed differences, we consider the effect of the transverse inhomogeneity of the wake of the leading body on the oscillatory motion of the trailing disk.

Key words: multiphase flow, multiphase and particle-laden flows, wakes/jets

1. Introduction

This paper investigates the hydrodynamical interaction at moderate Reynolds numbers of two identical solid axisymmetric bodies falling in tandem in a fluid otherwise at rest. The tandem configuration designates the situation in which the centres of gravity of the bodies are aligned with the average direction of motion of the bodies. A well-known feature of the interaction in this configuration is that the downstream body is entrained and accelerated by the wake of the leading body.

† Email address for correspondence: ern@imft.fr

In sports and biology, this phenomenon is at the origin of several types of cooperative behaviour between individuals. In multiphase flows, it may promote clusters or aggregates. It has therefore drawn considerable attention.

The first approach to analyse the entrainment phenomenon has been to consider the model case of two fixed bodies whose line of centres is parallel to the oncoming flow. The case of two fixed cylinders has been the subject of numerous numerical studies in two dimensions (Mittal, Kumar & Raghuvanshi 1997; Meneghini *et al.* 2001) and more recently in three dimensions (Carmo & Meneghini 2006). These studies demonstrated the reduction of the drag force on the second body. Mizushima & Norihisa (2005) noted in the case of an unsteady wake a significant reduction in drag for separations less than $\Delta_z = 3.3$ (Δ_z is the distance between the centres of gravity of the cylinders normalized with their diameter d). They also found that this configuration has a stabilizing effect on the flow: the critical Reynolds number for the transition from a steady to an unsteady wake increases from approximately 46 for an isolated cylinder to approximately 85 for two cylinders having a separation $\Delta_z = 2.5$.

The tandem configuration has also been studied for fixed three-dimensional objects, in particular for two spheres. The experimental studies of Tsuji, Morikawa & Terashima (1982) and Zhu, Liang & Fan (1994) focused on the evolution of the flow field and of the loads experienced by the bodies when their separation distance varies. The downstream sphere faces a reduced drag compared to an isolated sphere. The upstream sphere also sees its drag coefficient modified: it decreases or increases by approximately 15 % depending on the relative distance between the spheres. Zhu *et al.* (1994) proposed a dynamical model that includes the Basset force to simulate the velocity of a trailing sphere during the approach of two spheres. They found that the velocity of the trailing sphere increases linearly as the spheres get closer for $\Delta_z < 3$. More recently, Tsuji *et al.* (2003) obtained numerically that, as in the case of two-dimensional cylinders, the tandem configuration may stabilize the flow: the wakes are stationary and axisymmetric for Reynolds numbers up to 250 for a distance $\Delta_z = 3$ between the spheres, whereas for an isolated sphere the bifurcation corresponding to the loss of axial symmetry occurs at $Re_{c1} \approx 210$ (Natarajan & Acrivos 1993; Johnson & Patel 1999).

Yuan & Prosperetti (1994) in turn studied numerically the loads acting on two spherical bubbles for Reynolds numbers in the range 50 to 200. They found the existence of an equilibrium distance, denoted Δ_{z1}, that increases with the Reynolds number ($\Delta_{z1} = 3$ for $Re = 50$ and $\Delta_{z1} = 5.6$ for $Re = 200$). When $\Delta_z < \Delta_{z1}$ bubbles repel and otherwise they attract one another. They however pointed out that if the bubbles were free to move laterally relative to the incident flow, the trailing sphere would then deviate from the leading sphere wake. At this stage, it is interesting to recall that potential flow predicts that two spheres (or bubbles) placed one behind the other would repel. A first correction to this prediction that takes into account the effect of vorticity for an isolated bubble is the correction of Moore (1963). This viscous correction was used to predict the behaviour of a pair of spherical bubbles rising in a fluid at rest by Kok (1993*a*). Bubbles attract or repel one another depending on their separation distance and on the angle formed by the line of centres of the bubbles and the direction of the flow. He obtained that the stable position for two bubbles is when they come into contact, with the line passing through their centres of gravity perpendicular to their velocity. Kok (1993*b*) conducted an experimental study of two bubbles in a fluid free of contamination at $Re = 240$. He found results consistent with the foregoing: bubbles initially in tandem or slightly skewed, approach, turn

and get aligned horizontally, then they attract each other and coalesce. Contaminated bubbles behave as solid spheres: they touch and bounce back, eventually staying side by side. More recently, Hallez & Legendre (2011) simulated numerically the interaction between two fixed spherical undeformable bubbles. They included an additional correction that takes into account the effect of the wake on both the drag and the transverse force experienced by the second bubble when located in the wake of the first bubble and concluded that the stable final position for two bubbles rising in interaction would be the side-by-side configuration.

Jayaweera & Mason (1965) are to our knowledge the first to investigate the interaction between two disks freely falling in tandem for Reynolds numbers ranging from one to hundreds. In their experiment, the attraction between the two falling disks is visible for distances greater than 40 diameters. They also noted that when the trailing disk is close to the leading one, it may start to oscillate for $2 \leqslant \Delta_z \leqslant 3$. For smaller distances, both disks begin to oscillate. Furthermore, after contact the disks continue their fall together adopting a Y-configuration (the planes containing the disks form an angle of 30° for a Reynolds number of 100). For Reynolds numbers between 1 and 10, Jayaweera, Mason & Slack (1964) studied the interaction of two identical spheres freely falling in a fluid at rest. They observed that when the spheres are placed one behind the other, the trailing sphere is accelerated until the spheres meet, then the line joining their centres of gravity tends to become horizontal and the two spheres move away from each other. For Reynolds numbers of several hundreds, Fortes, Joseph & Lundgren (1987) studied experimentally the motion of two spheres in tandem. They described a dynamic scenario called 'drafting, kissing and tumbling' corresponding to the same events: the trailing sphere is drawn by the wake of the leading one, they meet and turn around each other. Then the scenario repeats possibly many times, the role of each sphere being reversed each time. Hu, Joseph & Crochet (1992) also observed the same chain of events numerically for two-dimensional cylindrical particles having Reynolds numbers of 30.

The goal of the present paper is to provide a quantitative description of the kinematics leading to the regrouping of the bodies and to improve our understanding of its coupling with the wake of the leading body, in particular in relation to the axial and transverse inhomogeneities of the wake. After describing the experimental setup and the numerical tool (§ 2), we present a general map showing the domains of existence for the different interaction behaviour of the two bodies as a function of their initial relative position (§ 3). We then focus on the tandem configuration, first for bodies having rectilinear paths (§ 4) and then for oscillatory paths (§ 5). In the first case, we propose a dynamical model for the trajectories of the bodies and investigate the relevance of the prediction provided by simulations for fixed bodies. In the second, we emphasize the effect of the interaction on the characteristics of the oscillatory motion and its strong dependence on the aspect ratio of the bodies. The paper ends with concluding remarks (§ 6).

2. The experimental and numerical tools

The bodies are released in a large glass tank (1.70 m high with a square cross-section of 0.4 m width) containing salted water of density $\rho_f = 1010$ kg m^{-3} and kinematic viscosity $\nu = 1.020$ mm^2 s^{-1} (see figure 1 of Fernandes *et al.* 2007). The bodies are short-length cylinders of density $\rho_s \simeq 1020$ kg m^{-3} (the density ratio between the bodies and the fluid is thus close to unity). Their diameters d (resp. heights h) range from 5 to 20 mm (resp. 1–5 mm). The aspect ratio $\chi = d/h$, which

	$\chi = d/h$	d (mm)	U_m (mm s^{-1})	Re	Path (isolated body)	Wake (isolated body)
Case 1	3	5.7	18.8	105	Rectilinear	Steady
Case 2	6	7.2	14.9	105	Rectilinear	Steady
Case 3	10	9	13.2	115	Rectilinear	Steady
Case 4	3	6.9	19.9	145	Rectilinear	Steady
Case 5	6	8.4	14.9	125	Rectilinear	Steady
Case 6	10	11	13.6	152	Rectilinear	Steady
Case 7	3	10.5	24.6	255	Oscillatory	Unsteady
Case 8	6	13.2	18.5	242	Oscillatory	Unsteady
Case 9	10	16	16.1	255	Oscillatory	Unsteady
Case 10	3	12	23.9	285	Oscillatory	Unsteady
Case 11	6	15	19.2	285	Oscillatory	Unsteady
Case 12	10	18	15.4	275	Oscillatory	Unsteady

TABLE 1. Characteristics of the bodies used for the experiments ('steady' means steady axisymmetric; 'unsteady' means unsteady with vortex shedding).

characterizes the anisotropy of the body, is chosen to be 3, 6 and 10, determined with an accuracy of $\pm 1\,\%$. The motion of the body depends on the Archimedes number Ar defined by $Ar = ((\Delta\rho/\rho_f)\, g\, r_{eq})^{1/2} r_{eq}/\nu$, where $\Delta\rho = |\rho_f - \rho_s|$, r_{eq} is the radius of the sphere having a volume equal to that of the body, and g is the gravitational acceleration. Note that Ar corresponds to a Reynolds number based on a gravitational velocity. Four characteristic values of Ar are considered here, approximately 35, 45, 85 and 110, allowing us to investigate both rectilinear and periodic motion (Fernandes *et al.* 2007). When a body is released alone in the tank, these values of Ar correspond to the Reynolds numbers $Re = (U_m\, d)/\nu \simeq 110$, 140, 250 and 280, where U_m is the mean vertical velocity of the isolated body. The characteristics of the bodies used for the experiments, along with their type of path and the nature of their wake when they are falling alone in the tank, are summarized in table 1.

In this study, we investigate the hydrodynamic interaction of two bodies that can be considered within experimental accuracy as identical. To investigate the case of bodies moving in tandem, the bodies are released consecutively through a 20 cm long tube. The diameter D of the release tube is at least twice the body diameter, in general 2.5–3 times larger ($D = 12$, 16, 22, 30 and 40 mm). The motion of the bodies is then recorded by means of two perpendicular travelling cameras. Recording of the body kinematics begins when the second body has left the release tube, and is at a distance from the first body corresponding to the field of view of the cameras (approximately 12 cm). At the exit of the tube, the bodies have a vertical velocity which is close to their terminal velocity in the isolated body case (approximately 90 % of U_m). In rectilinear motion, the bodies are falling broadside to the vertical and their inclination at the exit of the tube is weak (less than 3°), having no detectable effect on the recorded kinematics of the bodies. Bodies displaying periodic motion oscillate in the release tube with an amplitude comparable to that in the isolated body case. At the exit of tube, the inclination of the bodies varies from one experiment to the other but, as can be seen in figure 12(*a*) along with the differences in Δ_z and $\Delta_{h,m}$, this variation does not affect significantly the kinematics of regrouping of the bodies, and does not change the nature of the hydrodynamical interaction (attraction or repulsion) shown in figure 2. The image- and signal-processing techniques used to determine the time evolution of the coordinates of the centres of the bodies and the angles defining

the inclinations of their symmetry axes are described in detail in Fernandes *et al.* (2007). The use here of two PCO 2000 cameras of resolution 2048 pixel $\times$ 2048 pixel provides an accuracy of ± 0.06 mm for the position and of $\pm 0.75^\circ$ for the inclination.

To compare our results for freely moving bodies to the case of fixed bodies, we performed direct numerical simulations (DNS) of the flow past two fixed disks in a two-dimensional axisymmetric geometry at a Reynolds number of 100. We used the finite-volume code JADIM (see Legendre & Magnaudet 1998 for details and validation). We consider the case of two fixed disks placed in tandem in an incident flow aligned with their axes of symmetry. The simulations were performed for three aspect ratios ($\chi = 3$, 6 and 10) and for different relative distances Δ_z between the bodies ranging from 0.5 to 25 diameters (19 distances were tested for each aspect ratio). The computational domain extends over at least 35 diameters in the axial direction z and 20 diameters in the radial direction x. The grid was chosen according to the distance between the disks, comprising at least 174 meshes in the axial direction and 80 in the radial direction. For a given configuration, $\chi = 10$ and $\Delta_z = 3.25$, we checked that the mesh size (232×80 mesh) had no influence on the results by comparing them with those obtained with a finer mesh (415×98 mesh). The difference obtained for the drag coefficient C_d is less than 0.8 %. For $\chi = 10$, we also performed three-dimensional axisymmetric calculations for $\Delta_z = 2$ and $\Delta_z = 4$ in order to verify that the axisymmetric solution is stable and that the two-dimensional axisymmetric simulations are relevant. The difference obtained for the drag coefficient between the two-dimensional axisymmetric case and the three-dimensional case is for both distances less than 1 %.

3. Interaction behaviour as a function of the relative position

Depending on the initial relative position of the two disks, different interaction behaviour can be observed: attraction, repulsion and indifference. The relative position of the bodies is characterized by the vertical distance Δ_z and the horizontal distance Δ_h between the centres of gravity of the bodies, both normalized with the diameter d of the disks. Experiments for various relative initial positions were performed for Reynolds numbers in the range $Re \approx 100$–160 and for the three aspect ratios ($\chi = 3$, 6 and 10). Figure 1 shows some examples of the evolution of the distance separating the two disks in the plane (Δ_h, Δ_z). The initial relative position is identified by a black diamond. When the separation distance tends towards the point ($\Delta_h = 0$, $\Delta_z = 0$) it is regarded as an attraction case. If the distance does not vary significantly the case corresponds to a regime of independence, i.e. of no interaction. Bodies moving away from each other indicate a repulsion behaviour, as observed in the lower right of figure 1.

It should be noted that weak variations in the separation distance between the bodies are not necessarily due to their interaction but can also come from the dynamics of each body, as observed in Fernandes *et al.* (2007). The behaviour of the bodies might be influenced by weak residual movements in the liquid. Also, small differences in homogeneity, density and geometry between the bodies may lead to differences in their kinematics and thus to changes in their relative position. Insofar as the separation distance between the bodies does not vary significantly, it is unclear whether the changes are due to the interaction between the bodies or to perturbations in the path of each body. Therefore boundaries separating the different types of behaviour can be defined only with a horizontal uncertainty of $\pm 0.5d$.

The domains corresponding to the different interaction behaviour are mapped out in the plane (Δ_h, Δ_z) in figure 2. The initial relative positions of all tests are indicated

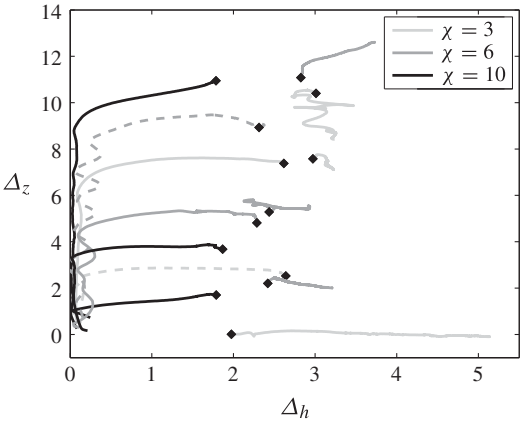

FIGURE 1. Examples of evolution of the separation distance between the bodies. Initial relative positions are indicated with black diamonds. Solid lines: cases 1–3 from table 1 and dashed lines: cases 4–6.

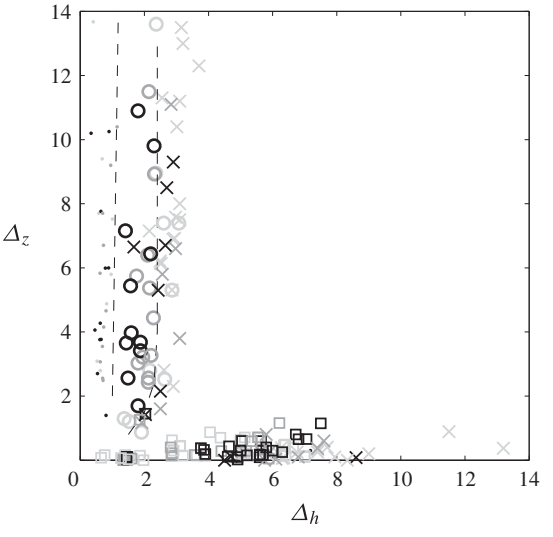

FIGURE 2. Domains of existence of the different interaction behaviour depending on the initial separation distance between the bodies: ○, weak attraction; ●, strong attraction; □, repulsion; ×, no interaction. Aspect ratios $\chi = 3$ (light grey), $\chi = 6$ (dark grey), $\chi = 10$ (black). (Cases 1–3 from table 1.)

with circles and dots for the attraction cases, squares for the repulsion cases and crosses for the cases of independence. Three domains are clear in figure 2. For $\Delta_z > 1$, a first region extending along the vertical coordinate and delimited by $\Delta_h = 2.5 \pm 0.5$ separates the situations of attraction from those of independence. This narrow region corresponds to a configuration of the bodies that will be termed 'in tandem' or 'in line' in what follows. In this configuration, the trailing body always catches up with the leading body. Our experiment allowed us to detect this phenomenon up to large vertical separation distances, $\Delta_z \simeq 14$. Furthermore, we distinguish two regions of

attraction called 'weak' and 'strong'. In the region of weak (resp. strong) attraction, the attraction leads to an increase of the vertical velocity of the trailing disk which is less (resp. larger) than 5 % of its vertical velocity in the absence of interaction (equal to the vertical velocity of the body when it is falling alone in the tank, U_m). The area corresponding to the situations of strong attraction is identified by the dots in figure 2 and corresponds to horizontal separations Δ_h less than 0.5 diameters. To the right of the attraction area, the domain of independence between the bodies, where no significant interaction is observed, extends along both Δ_h and Δ_z. The third region of interest is confined to $\Delta_z < 1$. In this area, the bodies are regarded as staying in the configuration called 'side by side'. For a horizontal distance $\Delta_h < 4.5$ we observe that the bodies repel one another. For distances spanning between 4.5 and 6, they never come closer. For distances greater than 6, the disks are independent of each other.

No significant difference in the boundaries separating the different regimes of interaction is observed when changing the aspect ratio and Reynolds number, in the ranges investigated. Yet these parameters have a strong impact on the kinematics of interaction. In particular, when thin bodies ($\chi = 6$ and 10) are falling in tandem, they eventually come into contact and continue their fall together adopting a Y-configuration described in Brosse & Ern (2011) and visible in the online supplementary movie available at http://dx.doi.org/10.1017/jfm.2014.407. In the case of thick bodies ($\chi = 3$), the disks separate after the first contact. In most cases, the trailing disk then goes past the leading disk and the sequence repeats as the latter now catches up with the former. However, after the second contact, the bodies always separate leading to the side-by-side configuration, where they eventually repel one another. In the case of thick bodies, attraction thus eventually leads to repulsion. The behaviour of thick bodies brings to mind the similar periodic sequence of attraction, contact and repositioning, called 'drafting, kissing and tumbling' by Fortes *et al.* (1987) for two spheres initially in tandem.

In the light of figure 2, two particular configurations come to the fore. While the side-by-side configuration and the associated repulsion behaviour are investigated in detail in the companion paper Ern & Brosse (2014), the focus of the present paper is on bodies falling in tandem and on the attraction behaviour. After the transient phase following the release of the bodies, we observed that the trailing body accelerates and that the two disks eventually meet. The aim of this paper is to characterize and model the phenomenon of entrainment experienced by the trailing body and driven by the wake of the leading body, both in the case of rectilinear and periodic paths and for three different aspect ratios of the bodies.

4. Body falling in tandem along straight paths

For a Reynolds number near 110, each disk follows a straight path when dropped alone. We observe that these bodies still follow a rectilinear path when they are interacting (i.e. they do not display any periodic oscillation in position or inclination). However, they accelerate along their paths, until they join. Since the vertical velocity of the bodies evolves in time, the mean fall velocity U_m and the Reynolds number Re used in this section are those of a disk dropped alone. Also, for the sake of readability, results shown in the figures of this section correspond to only one test for each aspect ratio, the results being reproducible between experiments (10 trials were performed for each aspect ratio and Re). In all the cases investigated in this section, the horizontal distance between the centres of gravity of the bodies Δ_h remains less than 0.5.

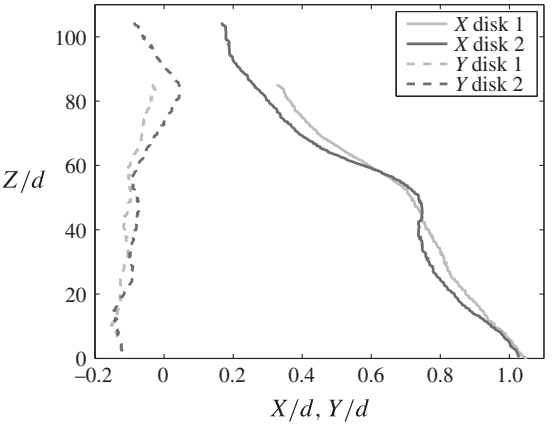

FIGURE 3. Example of the paths of two bodies projected in the vertical planes (X, Z) and (Y, Z). The coordinates are rescaled with the diameter d. (Case 1.)

4.1. *Paths of the bodies in the laboratory frame*

Figure 3 shows an example of the projections in the vertical planes, (X, Z) and (Y, Z), of the paths followed by two disks falling in tandem. The two disks exhibit a rectilinear vertical path, if we disregard the small horizontal drift occurring in this example in the plane (X, Z). The final horizontal drift of the bodies is always less than 3 % of the overall distance travelled vertically and varies from one experiment to the other, as it also happens for bodies falling alone (Fernandes *et al.* 2007). It is however noteworthy that the trailing disk presents a horizontal drift comparable to that of the leading disk, which is all the more remarkable given that this drift is weak. Furthermore, the mean direction of drift of the leading disk is opposite to the side where the trailing body is present. Two horizontal distances between the disks are relevant for the analysis of the interaction: the horizontal distance between the two centres of gravity Δ_h at a given time and the distance $\Delta_{h\,traj}$ between the two trajectories at a given height (figure 4*a*). The second definition determines the distance of the trailing disk from the path of the leading disk, and therefore provides a characterization of its position in the wake of the leading disk. We observe that the horizontal distance $\Delta_{h\,traj}$ between the two paths is generally lower than the distance between the centres of gravity Δ_h (figure 4*b*). Moreover, it seems that the disks tend to align vertically during their fall, Δ_h tending to decrease with time (figure 4*b*). All these observations point to a coupling between the drifts experienced by the two bodies through the wake of the leading body.

We now turn our attention to the effect of the interaction on the vertical motion of the bodies. Examples of the evolution in time of the vertical distance Δ_z between the centres of gravity of two disks are presented in figure 5(*a*). At first sight, this evolution seem independent of the aspect ratio, which is not exactly the case as will be shown later. The figure has to be read from right to left, the disks coming into contact at time $t = t_c$. Note that time has been made dimensionless using the inertial timescale d/U_m. We see that the vertical separation distance between the bodies decreases nonlinearly in time until they meet at $t = t_c$, indicating a non-uniform vertical velocity of the bodies. As a first characterization of the kinematics of approach of the two disks, the evolution of Δ_z can be approximated by

$$\Delta_z \sim (t_c - t)^{2/3} \quad \text{giving} \quad \Delta_U \sim \Delta_z^{-1/2}, \tag{4.1}$$

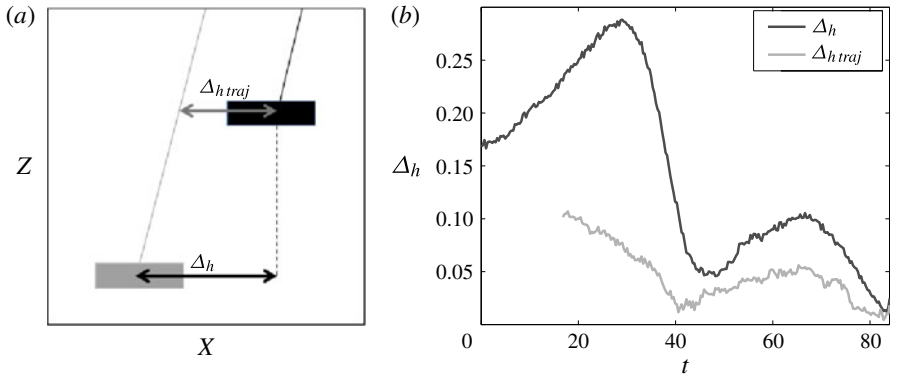

FIGURE 4. (*a*) Schematic representation of the horizontal distance between the centres of the bodies Δ_h and between the trajectories $\Delta_{h\,traj}$; (*b*) example of the evolution in time of the distances Δ_h and $\Delta_{h\,traj}$. (Case 1.)

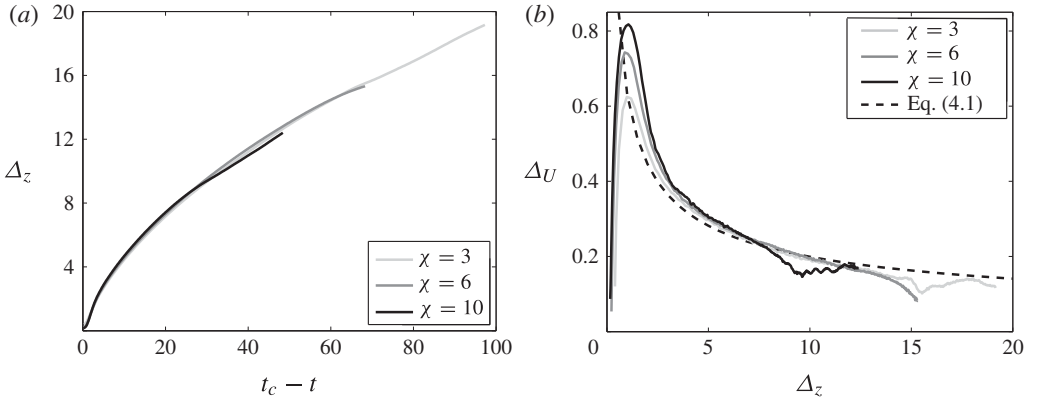

FIGURE 5. (*a*) Vertical distance between the two bodies Δ_z as a function of $t_c - t$; (*b*) corresponding relative velocity between the bodies $\Delta_U = \mathrm{d}\Delta_z/\mathrm{d}t$ as a function of Δ_z and comparison with (4.1) (dashed line). (Cases 1–3.)

where Δ_U is the velocity difference between the two disks. This is presented in figure 5(*b*) along with (4.1), showing that the latter is unable to describe the decrease in relative velocity occurring for distances less than two diameters, where it also misses the effect of the aspect ratio. We now investigate in more detail the evolution of the velocities of the bodies with their separation distance.

4.2. *Velocities of the bodies in the laboratory frame*

Figure 6(*a*) shows the evolution of the vertical velocity of the leading body, denoted U_{z1}, as a function of the vertical separation Δ_z between the bodies. Again, the figure reads from right to left, since Δ_z decreases with time – the bodies get closer until they meet – as shown previously. When the vertical separation is greater than four diameters, the leading disk has a constant velocity equal to its velocity in the absence of a second body. For sufficiently large separations, the kinematics of the leading disk thus seems unaffected by the presence of the trailing disk. However, whatever

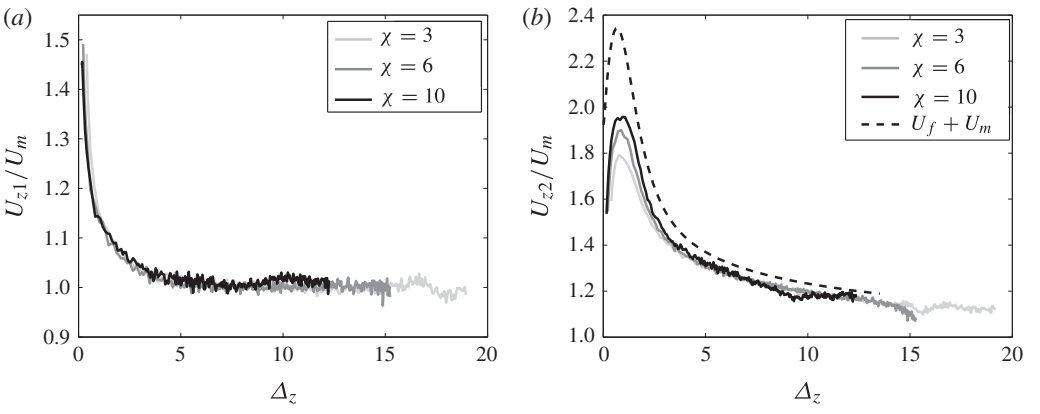

FIGURE 6. Velocity in the laboratory frame as a function of the vertical distance Δ_z between the bodies for (*a*) the leading body, U_{z1} and (*b*) the trailing body, U_{z2}. In (*b*), the dashed line corresponds to $U_f + U_m$, where U_f is the axial velocity in the wake of an isolated body, averaged over a disk of diameter d, obtained by numerical simulation for $\chi = \infty$ and $Re = 100$. The velocities are normalized with the vertical velocity U_m of the freely falling body in the absence of interaction. (Cases 1–3.)

the aspect ratio, at $\Delta_z \simeq 4$, the leading body starts to accelerate. When the bodies come into contact, the velocity of the leading body is 1.5 times larger than U_m, its velocity when falling alone. This suggests that the near wake of the leading disk is modified by the presence of the trailing disk beyond this separation distance. In particular, the recirculation zone is altered when it becomes confined between the two disks, as observed from wake visualizations (visible in Brosse & Ern (2011) and in the online supplementary movie).

Figure 6(*b*) shows the evolution of the vertical velocity U_{z2} of the trailing disk with Δ_z. The trailing disk has a vertical velocity always larger than that of the leading disk, even at large separation distances (15–20 body diameters). We can also see that U_{z2} increases as the bodies get closer until a maximum reached at about one diameter of vertical separation and decreases further beyond. While the evolution of U_{z2} is identical for all χ until a distance of approximately 2 diameters, the maximum depends on the aspect ratio of the bodies. For thin (resp. thick) bodies, it corresponds to approximately 2 (resp. 1.8) times the velocity of the isolated body. When the bodies come into contact, they have the same velocity, equal to 1.5 times the velocity of the isolated disk, whatever the aspect ratio. Figure 6(*b*) also presents with a dashed line the evolution of $U_f + U_m$, where U_f is the axial velocity of the fluid in the wake of an isolated disk, averaged over a disk of diameter d, obtained by numerical simulation for $\chi = \infty$ and $Re = 100$ (Auguste 2010; Auguste, Magnaudet & Fabre 2013). The evolution of the velocity in the wake of an isolated body shows clearly a trend similar to that measured for the trailing body. Furthermore, the numerical simulations by Fernandes *et al.* (2007) have shown that the maximum velocity of the fluid in the recirculation zone of an isolated disk is larger for thin disks than for thick disks. These results suggest that the attraction phenomenon is essentially governed by the axial evolution of the fluid velocity in the wake of the first body. In the next section, we use this idea to elaborate a model for the entrainment undergone by the trailing body. We also explore how far the results from numerical simulations for two fixed bodies in tandem can allow prediction of the kinematics observed for the two freely moving bodies.

4.3. *Some theoretical and numerical considerations*

4.3.1. *A simple model for the entrainment phenomenon*

The aim of this section is to obtain a prediction for the velocities of two bodies falling in tandem along rectilinear paths. We denote U_{s1} and U_{s2} the vertical velocities of the leading and trailing bodies to be determined with the model. For each body, a one-dimensional model along the vertical z axis is written using the formulation which applies to the case of an inclusion small compared to the inhomogeneity scales of the surrounding flow (Magnaudet 1997; Magnaudet & Eames 2000). We consider that the flow $U_{f1}(z, t)$ induced by the leading body has an impact on the motion of the trailing body by changing the drag force and by generating an inertial force related to the spatial variation of the flow. For the leading disk, we only take into account the deficit in drag related to the flow $U_{f2}(z, t)$ generated by the motion of the trailing body. We therefore have

$$(m_s + m_a)\frac{\mathrm{d}U_{s1}}{\mathrm{d}t} = \frac{1}{2} C_d\, \rho_f\, S\, |U_{f2} - U_{s1}|\, (U_{f2} - U_{s1}) + (m_s - m_f)\, g, \tag{4.2}$$

$$(m_s + m_a)\frac{\mathrm{d}U_{s2}}{\mathrm{d}t} = \frac{1}{2} C_d\, \rho_f\, S\, |U_{f1} - U_{s2}|\, (U_{f1} - U_{s2}) + (m_f + m_a)\left.\frac{\mathrm{D}U_{f1}}{\mathrm{D}t}\right|_p + (m_s - m_f)\, g \tag{4.3}$$

where $m_a = \rho_f d^3(1 + 0.5\chi^{-1/2})/3$ is the added mass coefficient along the axial direction of a disk of aspect ratio χ (Fernandes *et al.* 2008), $m_s = \rho_s \vartheta$ and $m_f = \rho_f \vartheta$ where $\vartheta = Sh$ is the volume of the body with $S = \pi d^2/4$, and C_d is the drag coefficient of the isolated body such that $C_d \rho_f S U_m^2/2 = |m_s - m_f| g$. For the equation of the trailing body, in a coordinate system linked to the centre of gravity of the leading body, we take $U_{f1}(\Delta_z, t) = U'_{f1}(\Delta_z)\, U_{s1}(t)$ where U'_{f1} is the dimensionless axial velocity in the wake of an isolated disk (with $\chi = \infty$) in uniform rectilinear motion at $Re = 100$, averaged at each z over the surface of the disk, obtained by numerical simulation (Auguste 2010). The particulate derivative of the fluid velocity at the position of the body then is

$$\left.\frac{\mathrm{D}U_{f1}(\Delta_z, t)}{\mathrm{D}t}\right|_p = \frac{\partial U_{f1}(\Delta_z, t)}{\partial t} + (U_{f1}(\Delta_z, t) - U_{s1}(t))\, \frac{\partial U_{f1}(\Delta_z, t)}{\partial \Delta_z}. \tag{4.4}$$

In the same way, we take for the leading body in the moving frame of the trailing body $U_{f2}(\Delta_z, t) = U'_{f2}(\Delta_z)\, U_{s2}(t)$ where U'_{f2} is the dimensionless axial velocity of the fluid upstream of a single disk (with $\chi = \infty$) in uniform rectilinear motion at $Re = 100$, averaged at each z over the surface of the disk (Auguste 2010). Using the velocity scale U_m and the timescale d/U_m to render the equations dimensionless, the system becomes

$$\left(\frac{\rho_s}{\rho_f} + A\right)\frac{\mathrm{d}\,U_{s1}}{\mathrm{d}\,t} = \frac{1}{2} C_d\, \chi\, \left[|U_{f2} - U_{s1}|(U_{f2} - U_{s1}) + 1\right], \tag{4.5}$$

$$\left(\frac{\rho_s}{\rho_f} + A\right)\frac{\mathrm{d}U_{s2}}{\mathrm{d}t} = (1 + A)\left.\frac{\mathrm{D}U_{f1}}{\mathrm{D}t}\right|_p + \frac{1}{2} C_d\, \chi\, \left[|U_{f1} - U_{s2}|(U_{f1} - U_{s2}) + 1\right], \tag{4.6}$$

where $A = m_a/m_f$. We solve the coupled equations (4.5)–(4.6) using a Runge–Kutta algorithm of order 4, with the initial conditions $\Delta_{z,0} = 11$, $U_{s1,0} = 1$ and $U_{s2,0} = 1.15$,

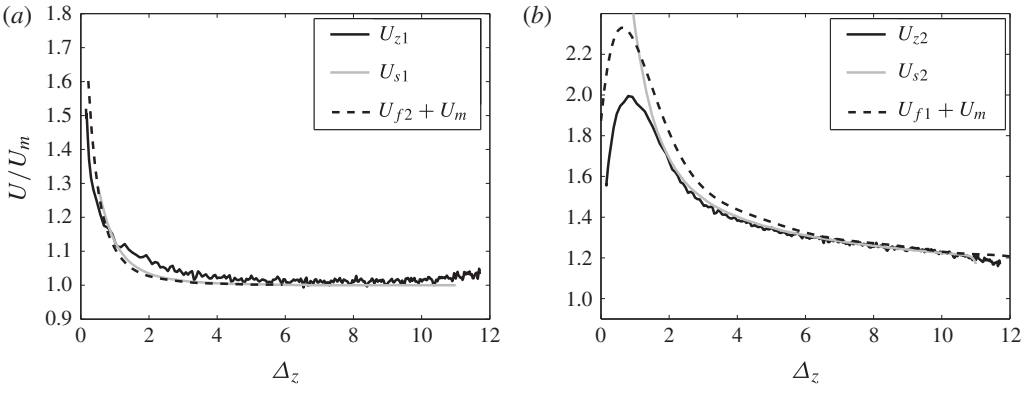

FIGURE 7. Comparison in the laboratory frame of the evolution of the vertical velocities of the disks with Δ_z for (*a*) the leading body and (*b*) the trailing body, obtained experimentally and with the model. (Case 3.)

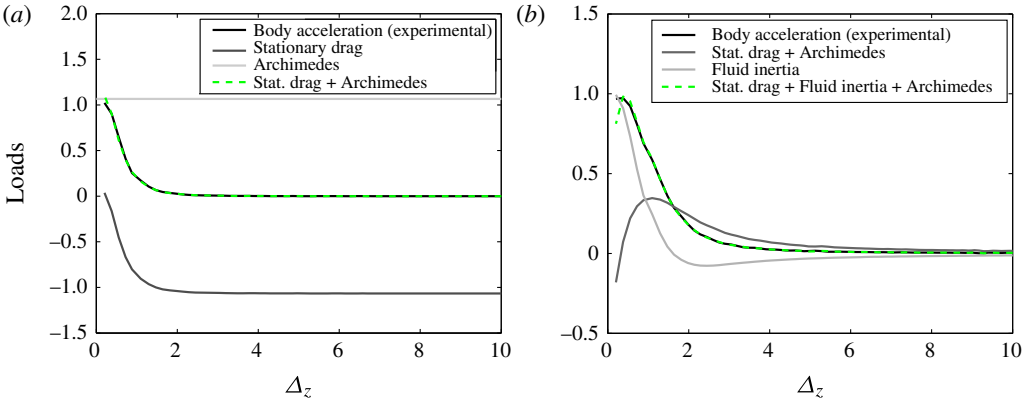

FIGURE 8. (Colour online) Forces rescaled by $(m_s + m_a)\, U_m^2/d$ obtained (*a*) for the leading body, (*b*) for the trailing body. (Case 3.)

and with $C_d = 1.26$ (corresponding to the drag coefficient of an isolated body with aspect ratio $\chi = 10$ and $Re = 100$). Figures 7(*a*) and 7(*b*) compare the velocities U_{z1} and U_{z2} measured experimentally to the velocities U_{s1} and U_{s2} predicted by the model for each body. We observe that the model provides a good approximation of the evolution of the velocity of the leading body with Δ_z (figure 7*a*). As regards the trailing disk, the model reproduces the body acceleration for separations greater than 1.5 diameters (figure 7*b*).

Figure 8 shows the evolution with Δ_z of the various loads acting on the bodies in the model. For the leading disk (figure 8*a*), when the vertical separation between the bodies is greater than four diameters, the drag force balances the Archimedes force, as in the isolated body case. For distances $\Delta_z < 4$, the absolute value of the drag term decreases due to the upstream flow of the trailing disk and drives the acceleration of the leading disk. As shown in figure 8(*b*), the acceleration of the trailing body is mainly provided by the decrease of the absolute value of the steady drag term and is slightly moderated by the term proportional to the fluid particulate derivative (4.4). For the two bodies, the model fails for $\Delta_z < 1.5$. As can be seen from the

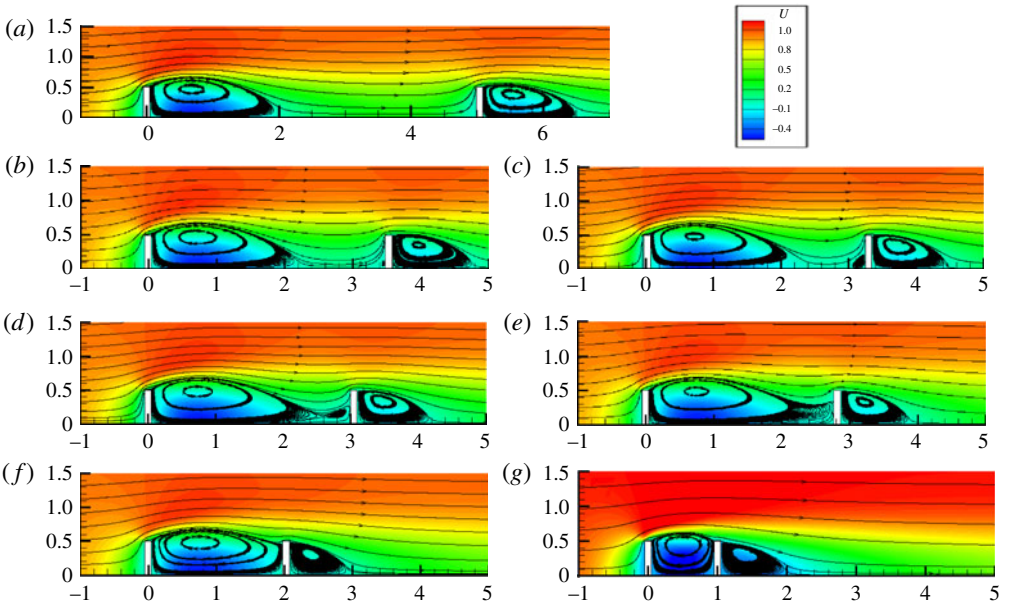

FIGURE 9. (Colour online) The wake of two fixed bodies placed in tandem with aspect ratio $\chi = 10$ at $Re = 100$: streamlines and axial velocity obtained by numerical simulation for different relative distances: (*a*) $\Delta_z = 5$, (*b*) 3.5, (*c*) 3.25, (*d*) 3, (*e*) 2.75, (*f*) 2, (*g*) 1.

dye visualizations presented in Brosse & Ern (2011) and in the online supplementary movies, when the bodies are close, a complex interaction occurs between the liquid motions induced by the bodies, which is not accounted for by the model.

4.3.2. *Numerical prediction for two fixed disks in tandem*

The determination by numerical simulations of the hydrodynamical loads acting on two fixed bodies placed in an oncoming flow is generally the prevalent approach to obtain a prediction for the behaviour of freely moving bodies. To investigate the suitability of this approach, we performed numerical simulations of the flow about two fixed disks placed in tandem at different distances Δ_z, for $Re = 100$ and three aspect ratios ($\chi = 3$, 6 and 10). The distances separating the fixed disks vary from $\Delta_z = 0.5$ to 25. For each separation distance, we determine the loads acting on the bodies. The evolution of the loads as a function of the separation distance is then used to estimate what would be the accelerations of the bodies if they were free to move.

Figure 9 plots the streamlines and the axial velocity of the flow for various distances Δ_z between the bodies. As a complement, figure 10 shows the axial velocity U_{fz} of the flow past the two fixed disks taken on the symmetry axis of the disks for different relative distances Δ_z. For comparison, the flow about an isolated body is also drawn with a dashed line in figure 10. The first body is placed at the origin. The position of the second body for each separation distance corresponds to the plateau at zero velocity. The velocity at upstream infinity is set to one; negative velocities at the rear of each body correspond to the recirculation zones. For separations Δ_z larger than 3.5 (figure 9*a*) the near wake of the first disk is very similar to that of an isolated disk with a recirculation zone that extends two diameters behind the disk.

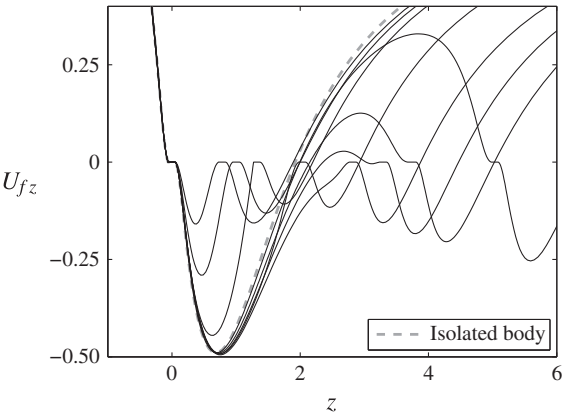

FIGURE 10. Evolution of the axial velocity U_{fz} of the flow about two fixed disks along the direction z (corresponding to the symmetry axis of the bodies), obtained by numerical simulations for different separation distances Δ_z between the disks, for $\chi = 10$ and $Re = 100$. The flow is directed towards the positive z values and equals 1 at upstream infinity. The first body is placed at the origin. The position of the second body in each case corresponds to the plateau at zero velocity.

For separations Δ_z in the interval [3.25, 3.5] the recirculation zone of the first body is slightly stretched. Moreover, a secondary recirculation zone develops in front of the second body (figure 9*b*,*c*) due to the deficit in flow velocity induced on the axis by the wake of the first body. When the bodies are slightly closer than $\Delta_z = 3$ (figure 9*d*) the two recirculation zones come into contact and merge giving rise to a larger recirculation region that entirely fills the gap between the two bodies. As the bodies separation decreases from 2.75 to 1 diameters (figure 9*e*–*g*), this recirculation zone is correspondingly constricted. These results are consistent with the two-dimensional numerical simulations by Mizushima & Norihisa (2005), which observed that for a Reynolds number of 60 the recirculation zone between the two cylinders could be stretched or compressed depending on the relative distance between the cylinders. Finally, note that for all Δ_z, the length of the recirculation zone of the second disk is reduced compare to that of an isolated body and decreases in intensity until about $\Delta_z = 2$.

For each separation distance, we determine from the numerical simulations the magnitude of the drag force acting on each body. Figure 11(*a*) shows the evolution of the drag coefficient for each disk, denoted C_{d1} and C_{d2}, as a function of the distance Δ_z between the bodies for $\chi = 3$ and $Re = 100$. The figure presents the ratios between C_{d1} and C_{d2} with respect to the value C_{d0} for an isolated disk. The drag coefficient of the first body is close to C_{d0}. We observe that the presence of the second body changes the forces acting on the first body only for distances less than 5 diameters. The drag coefficient of the second body is always smaller than C_{d0} and decreases as the disks are set closer together. These results are in agreement with the experimental study of Zhu *et al.* (1994) for two spheres in tandem at $Re = 106$, also shown in figure 11(*a*).

We now consider the quasi-static motion of a body resulting from the balance between the Archimedes force and a drag force evolving with Δ_z according to the results provided by the numerical simulations. The resulting velocities of the bodies,

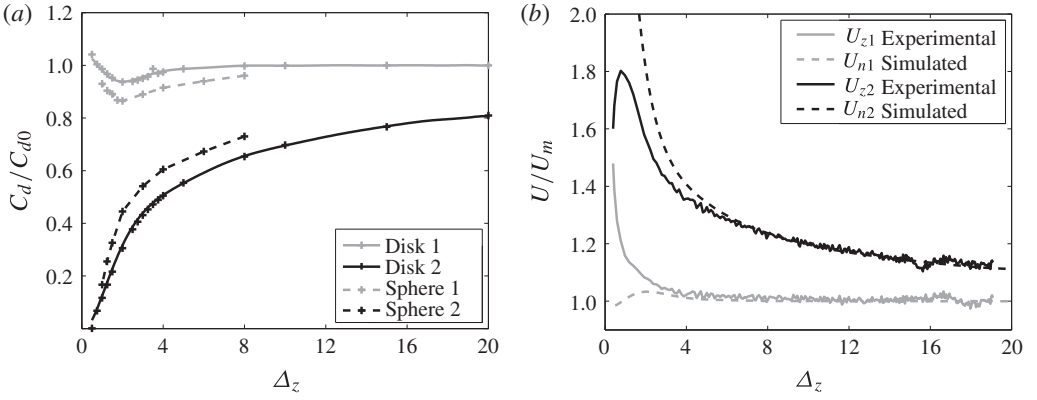

FIGURE 11. (*a*) Evolution of the drag coefficient C_d/C_{d0} of the first and second disks (for $\chi = 3$, $Re = 100$, $C_{d0} = 1.255$) as a function of Δ_z. The dashed lines correspond to the case of spheres obtained experimentally at $Re = 106$ by Zhu *et al.* (1994). (*b*) Comparison of the evolution of the vertical velocities of the bodies with Δ_z, obtained experimentally and from the numerical simulations for fixed bodies. (Case 1.)

U_{n1} and U_{n2}, are then given by

$$U_{ni}^2 = \frac{F_g}{\frac{1}{2} C_{di}\, \rho_f\, S} \quad \text{with } F_g = \frac{1}{2}\, C_{d0}\, \rho_f\, S\, U_m^2 \tag{4.7}$$

so that

$$U_{ni}(\Delta_z) = \sqrt{\frac{C_{d0}}{C_{di}(\Delta_z)}}\, U_m \quad \text{for } i = 1, 2. \tag{4.8}$$

Recall that the drag coefficient C_{d0} and the velocity U_m considered are the values for an isolated disk at the same Reynolds number. Figure 11(*b*) compares the experimental velocities U_{z1} and U_{z2} of the freely moving bodies with those found using this method. The quasi-static prediction matches the experimental kinematics of the disks with a good approximation for relative distances $\Delta_z > 5$ with differences smaller than $\pm 3\,\%$, while it overestimates the acceleration of the trailing body and underestimates that of the leading body for $\Delta_z < 5$. For these small separation distances, the quasi-static approach is no longer valid as the unsteady terms associated with the solid and the fluid motion are no longer negligible with respect to the steady drag component. Also, the dynamics of the interaction of the wake vortices are not properly taken into account in the numerical simulations with fixed disks. In the wake visualizations performed for freely moving bodies with $\chi = 3$ and $\chi = 10$ and provided in Brosse & Ern (2011) (see also the online supplementary movies), a completely different behaviour from that of figure 9 is observed for freely moving bodies for distances $\Delta_z < 4$. In particular, as the separation distance decreases, instead of remaining confined between the two disks, the recirculation region of the leading disk stretches and encompasses the trailing body and its wake, leading to a leap-frog behaviour between the two recirculation regions.

5. Bodies falling in tandem with periodic paths

We now consider the case of disks having periodic paths. When the bodies are falling alone, their mean vertical velocities correspond to Reynolds numbers ranging

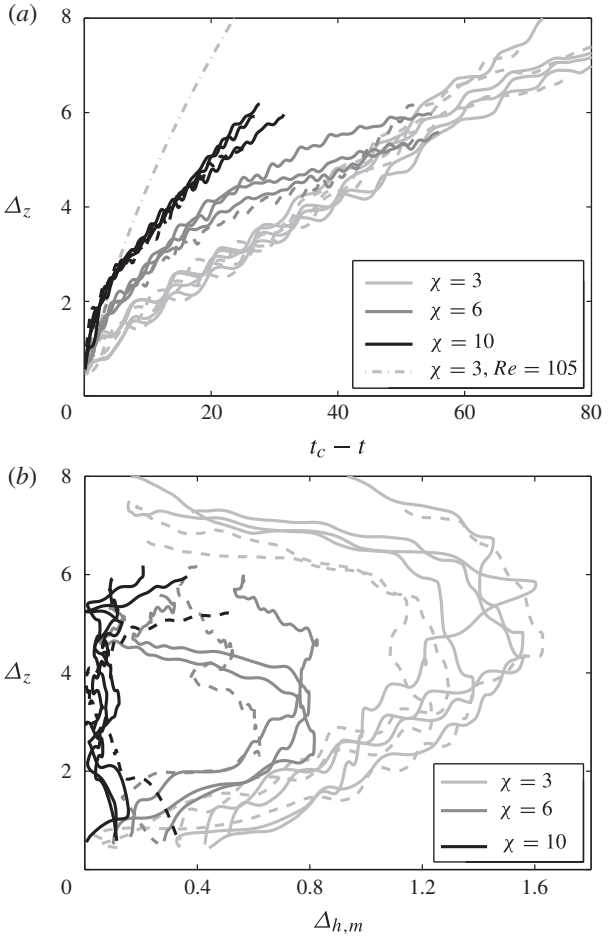

FIGURE 12. Vertical distance separating the bodies Δ_z as a function of (*a*) time $t_c - t$ and (*b*) the mean horizontal distance between the bodies $\Delta_{h,m}$ (solid lines: cases 7–9; dashed lines: cases 10–12; dashed-dotted line in (*a*) case 1).

from 240 to 285 (cases 7–12 from table 1). In all cases, we observe that the trailing disk catches up with the leading disk, as in the previous records for rectilinear paths. Again, thick bodies ($\chi = 3$) tend to separate after they meet, while thinner bodies ($\chi = 6$ and 10) stay together (Brosse & Ern 2011). However, for isolated bodies having periodic paths, the impact of the interaction on the kinematics of the trailing body is twofold: an increase of its mean vertical velocity and a modification of the characteristics of its oscillatory motion. The next two subsections investigate these two effects.

5.1. *Entrainment by the wake*

Figure 12(*a*) shows the evolution of the vertical distance Δ_z between the disks as a function of the dimensionless time $t_c - t$ for the three aspect ratios. At variance with the case of rectilinear paths, the kinematics of oscillating bodies strongly depends on the aspect ratio. In fact, the slope of the curves is higher for the thin disk

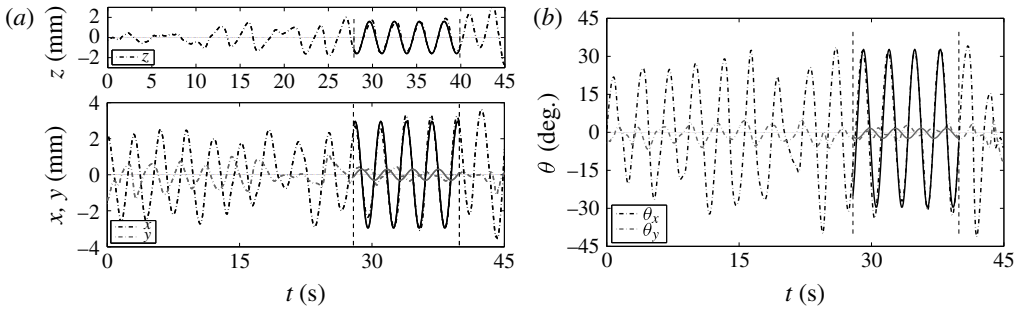

FIGURE 13. Example of the oscillations of the trailing body after signal processing: (*a*) oscillations of the centre of gravity of the body in the vertical direction relative to a mean vertical evolution (top) and in a horizontal plane (bottom); (*b*) angles of inclination of the axis of symmetry of the body relative to the vertical. Solid black lines represent the fitted part of the curves. (Case 7.)

($\chi = 10$) indicating that they are closing together faster than thick disks ($\chi = 3$). For comparison, the evolution corresponding to the straight paths is plotted with a dashed-dotted line in figure 12(*a*). Whatever the aspect ratio, closing is slower for oscillatory paths than for rectilinear paths.

To investigate more deeply the effect of the aspect ratio, we look at the evolution of the horizontal distance between the centres of gravity of the bodies, Δ_h. Due to the horizontal oscillations of the disks, Δ_h also oscillates. For clarity, we focus on its mean component, denoted $\Delta_{h,m}$ (where $\Delta_{h,m} = \left((\hat{x}_2 - \hat{x}_1)^2 + (\hat{y}_2 - \hat{y}_1)^2\right)^{1/2}$ and where $\hat{x}_i$ and $\hat{y}_i$ are the horizontal coordinates of a body in the principal frame of oscillations as defined in Fernandes *et al.* 2007, $i = 1$ or 2 each standing for one body). Figure 12(*b*) shows the evolution of $\Delta_{h,m}$ associated with the evolution of Δ_z for several trials. We observe that the thin trailing body ($\chi = 10$) remains aligned vertically with the thin leading disk, the horizontal distance $\Delta_{h,m}$ being always less than 0.3. On the contrary, for thick bodies ($\chi = 3$) the trailing body first drifts away from the centre of the wake of the leading body ($\Delta_{h,m} > 1.2$ for $\Delta_z > 4$) but is later captured at smaller Δ_z, eventually joining the leading disk. As they travel in a flow area of less intense velocity, they benefit from a weaker entrainment and their approach is slower. Thin trailing disks travel in the central zone of the wake where larger fluid velocities speed their approach. The horizontal ejection observed for the thick trailing disk at large Δ_z might be related to the way the body evolves along its path. Placed in a shear zone of decreasing velocities as in figure 4(*a*), the body undergoes a torque that leads it to rotate counterclockwise around one diametrical direction. When a thick disk is tilted, it tends to move in the direction of its symmetry axis (Fernandes *et al.* 2005), in this case away from the centreline of the wake of the leading disk. On the contrary, for the same rotation, a thin disk tends to move sideways, in this case towards the centreline of the wake.

5.2. *Characteristics of the oscillations*

In this section, we explore the characteristics of the oscillatory motion of the two disks. Figures 13(*a*) and 13(*b*) show an example of the oscillations in time of the position and the inclination of the trailing body after signal processing. This consists of removing the average drift and determining the principal frame of the oscillations

(see Fernandes *et al.* 2007 for the details of the method). We see that the signals still display irregular oscillations and that the amplitude and frequency of the oscillations of the position and of the orientation are not constant over time. In particular, one or two temporal periods before the bodies come into contact, the interaction leads to a change in the oscillations of the bodies that depends on the way they are getting nearer. However, a few periods before (corresponding to about $2 < \Delta_z < 6$) the mean vertical velocities of the leading and trailing bodies (respectively $U_{m,B1}$ and $U_{m,B2}$) are almost constant and so is the mean horizontal distance $\Delta_{h,m}$ between the bodies. Also, the order of magnitude of the frequency and of the amplitude of the oscillations in position and orientation can be determined by fitting the signals (as shown with black solid lines in figure 13*a*,*b*). In this range of separation distances, a Reynolds number for both the leading and the trailing body can be defined based on their velocities $U_{m,B1}$ and $U_{m,B2}$. In figure 14, these Reynolds numbers are all called Re, as is the Reynolds number of the isolated body, but the legend indicates which body is considered (B1 for leading body and B2 for the trailing body). In the same way, a Strouhal number, denoted St for all cases, is defined for the isolated body, for the leading body and for the trailing body, using their frequencies of oscillation, their diameter and their mean vertical velocities.

Figure 14 shows that the kinematics of the leading body (open symbols) is not significantly different from the isolated body case (solid lines), whereas the case of the trailing disk (filled symbols) deserves a closer examination. The Strouhal number of the trailing disk follows the same evolution as that of an isolated body for aspect ratios $\chi = 3$ and $\chi = 6$ but tends to decrease for thinner bodies $\chi = 10$ (figure 14*a*). The amplitudes of oscillation of the horizontal position of the trailing body are larger than those of the isolated body at the same Reynolds number (figure 14*b*), increasingly so as the body gets thinner. At the same time, the amplitudes of the angular oscillation of the trailing body (figure 14*c*) seem to be less affected by the interaction. For the same amplitude of inclination, the trailing body performs a greater horizontal motion and the phase difference between the horizontal velocity and the inclination (figure 14*d*) is slightly modified. The increase in amplitude of horizontal oscillation is even more significant as the nature of the path has also been affected by the interaction. As can be seen in figure 14(*e*), the eccentricity of the path of the trailing body is much larger than that of the isolated body, whatever the aspect ratio. The path can no longer be considered as a planar zigzag but approaches a helical shape, the eccentricity being in most cases half or more.

An additional remarkable feature is the increase in the amplitude of vertical oscillation of the trailing body with aspect ratio $\chi = 3$. In the isolated body case, the amplitude of the oscillation in vertical position is negligible for a thick body ($\chi = 3$). This amplitude is here multiplied by a factor ten for this aspect ratio, exceeding the amplitudes for the aspect ratio $\chi = 10$, which appear unaffected by the interaction (figure 14*f*). Furthermore, for the aspect ratio $\chi = 3$, the frequency of the vertical oscillation is the same as that of the horizontal oscillation, whereas for an isolated body it is doubled. To investigate the origin of the vertical oscillation we plot in figure 15 the vertical velocity of the trailing body U_{z2} as a function of the distance between the centre of gravity of the trailing body and the path of the leading body $\Delta_{h\,traj}$ (represented in figure 4*a*). Over a period, we observe that when the trailing body gets closer to the centreline of the wake of the leading body, it accelerates. Likewise, when it retreats, it decelerates. This result indicates that the transverse inhomogeneity of the flow in which the trailing body is travelling drives the large oscillations of its vertical velocity.

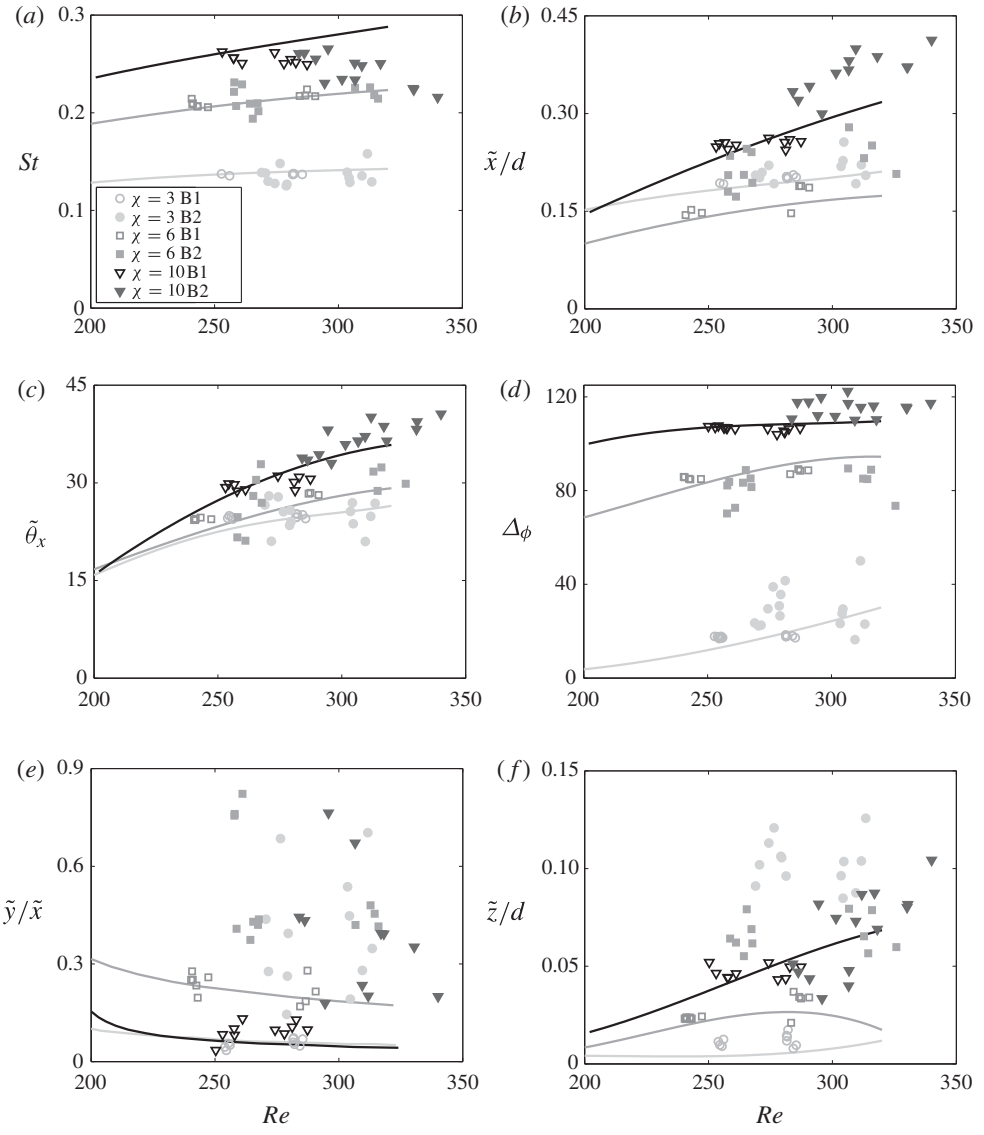

FIGURE 14. Characteristics of the oscillations of bodies falling in tandem as a function of the Reynolds number: (*a*) Strouhal number, (*b*) amplitude of oscillation of the horizontal position, (*c*) amplitude of the inclination, (*d*) phase difference between the horizontal velocity and the inclination, (*e*) eccentricity of the path, (*f*) amplitude of oscillation of the vertical position. The solid lines represent the mean values for isolated disks: light grey $\chi = 3$, dark grey $\chi = 6$, black $\chi = 10$. The leading body is labelled B1 and the trailing body B2.

A different, yet particularly interesting, situation is the case of disks having rectilinear paths with Reynolds numbers slightly below the threshold of path instability in the absence of interaction. For these *Re*, we observe a great variability in the kinematics for the same disks, especially for $\chi = 3$ and $\chi = 6$, without being able to determine its cause. We observe that the path of the trailing disk can be either stable

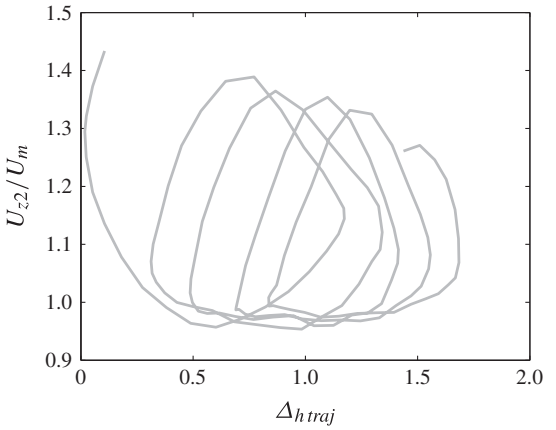

FIGURE 15. Vertical velocity of the trailing disk (relative to its velocity U_m in the absence of interaction) as a function of the distance between the trajectories of the bodies $\Delta_{h\,traj}$. The curve evolves from right to left as time increases. (Case 7.)

or destabilized, i.e. the body can lose its rectilinear motion and start to oscillate. As observed previously, in the cases where the trailing body oscillates, its approach is slower. In the following, we will focus our attention on the oscillatory cases. For a thick body with $\chi = 3$, we observe that the oscillations present the same features as those previously described at higher Reynolds numbers for a trailing body having a periodic path. Moreover, we observe that these oscillations are triggered when the entrainment provided by the wake of the leading body drives the trailing disks at Reynolds numbers that exceed the threshold for path instability for isolated disks. For thin disks ($\chi = 10$), the oscillation occurs at lower Reynolds number than the threshold leading to large-amplitude path oscillations of the body (Fernandes *et al.* 2007). However, the amplitudes of oscillation in position are larger than those observed numerically for an isolated disk at the same Reynolds number in the so-called 'A-regime' (Ern *et al.* 2012; Auguste *et al.* 2013), where paths of very small amplitude were observed only numerically (displacements here of approximately 0.15 diameters compared to displacements of approximately 0.015 diameters for the isolated body in the simulations by Auguste (2010) and Auguste *et al.* (2013)). At the same time, the oscillation frequency corresponds to the Strouhal numbers of the modes of the A-regime, $St \approx 0.12$, which is close to the Strouhal number of the natural instability of the wake of the fixed body. For thin disks, the wake of the leading body seems to destabilize the path of the trailing body by destabilizing its wake and the induced oscillations seem to mainly correspond to an amplification of the modes of the A-regime.

6. Conclusion

We consider the interaction of two identical disks falling in a fluid otherwise at rest. Depending on the relative position of the bodies, different interaction behaviour is observed. Bodies in tandem with a horizontal distance less than 0.5 diameters are attracted even for vertical separation distances Δ_z as large as 14 diameters, so that the trailing body eventually catches up with the leading body. For $\Delta_z < 1$, bodies falling side by side repulse one another for horizontal separation distances less than

4.5 diameters. For the other relative positions, the bodies seem independent of the presence of the other body and no change in their path is observed relative to the isolated body case.

We investigate in detail the kinematics of the bodies in the tandem configuration as a function of the Reynolds number and of the aspect ratio of the bodies. For disks following a straight path, the kinematics leading to the regrouping of the bodies is independent of the aspect ratio for $\Delta_z \geqslant 2.5$. We observe that the leading body is unaffected by the presence of the trailing body when $\Delta_z \geqslant 4$, beyond which it starts to accelerate. The trailing body experiences, on the contrary, an acceleration even far away from the leading disk. Its velocity is already 20 % larger than its velocity in the absence of interaction for $\Delta_z \simeq 10$ and reaches about twice this velocity for $\Delta_z \simeq 1$.

To analyse the key role of the wake of the leading body on the entrainment experienced by the trailing body, we propose a model for the velocities of the bodies that includes a stationary drag force as well as an inertia force, both dependent on the axial evolution of the flow about a freely moving single body. The model correctly reproduces the experimental kinematics for separations $\Delta_z > 1.5$. In addition, we performed numerical simulations for two fixed disks placed in tandem in an oncoming flow to determine the evolution of their drag coefficient as a function of their separation distance. Using these evolutions to predict the motion of the bodies yields satisfactory results only for disks sufficiently far apart, $\Delta_z > 5$. For smaller separation distances, the numerical prediction overestimates the acceleration of the trailing body, while that of the leading body is underestimated. As can be seen in Brosse & Ern (2011) and in the supplementary online movies, dye visualizations of the wakes of freely moving bodies indicate a completely different behaviour of the recirculation regions for freely moving bodies than in the case of fixed bodies, shedding light on why the fixed body approach is unable to reproduce the kinematics of the freely moving bodies at small Δ_z.

For Reynolds numbers close to the threshold of path instability, the interaction may cause the trailing disk to oscillate and the characteristics of the oscillation then strongly depend on χ. For thick bodies, $\chi = 3$, the entrainment results in an increase of the vertical velocity, that may correspond to Reynolds numbers larger than the threshold of path instability, thus giving rise to oscillations. For thin bodies, $\chi = 10$, the onset of oscillations seems to be caused by the inhomogeneity of the wake of the leading body that destabilizes the wake of the trailing body, inducing oscillations at lower Strouhal numbers.

We show that the kinematics leading to the regrouping of the bodies depends on the Reynolds number, being faster for the rectilinear paths than for periodic paths. However, in the case of periodic paths, the interaction not only leads to a gain in vertical velocity for the trailing body but also induces significant changes in the characteristics of its oscillatory motion. In particular, the oscillations of the trailing body are amplified, displaying amplitudes in the horizontal plane or along the vertical direction markedly larger than those observed for isolated bodies at the same Reynolds numbers. We investigate how the transverse inhomogeneity of the wake of the leading body may contribute to this behaviour. For bodies with oscillatory paths, the kinematics leading to the regrouping of the bodies depends on the aspect ratio. Thin trailing disks stay centred in the wake of the leading disk and approach the leading disk faster than thick disks that drift away from the wake centreline, thereby benefiting from a weaker entrainment.

Finally, we observe that after the bodies meet, thin disks ($\chi = 6$ and 10) continue their fall together whatever the Reynolds number, adopting the Y-configuration

investigated in Brosse & Ern (2011). On the contrary, thick disks ($\chi = 3$) tend to separate after contact so that they eventually fall side by side, a configuration considered in Ern & Brosse (2014).

Acknowledgements

The authors warmly thank F. Auguste, D. Fabre and J. Magnaudet for providing the numerical code and a stimulating working environment. They are also grateful to G. Ehses, H. Ayroles and S. Cazin for the technical support provided for the experiments.

Supplementary movies

Supplementary movies are available at http://dx.doi.org/10.1017/jfm.2014.407.

REFERENCES

AUGUSTE, F. 2010 Instabilités de sillage générées derrière un corps solide cylindrique, fixe ou mobile dans un fluide visqueux. PhD thesis, Université Paul Sabatier, Toulouse, France.

AUGUSTE, F., MAGNAUDET, J. & FABRE, D. 2013 Falling styles of disks. *J. Fluid Mech.* **719**, 388–405.

BROSSE, N. & ERN, P. 2011 Paths of stable configurations resulting from the interaction of two disks falling in tandem. *J. Fluids Struct.* **27** (5–6), 817–823.

CARMO, B. S. & MENEGHINI, J. R. 2006 Numerical investigation of the flow around two circular cylinders in tandem. *J. Fluids Struct.* **22** (6–7), 979–988.

ERN, P. & BROSSE, N. 2014 Interaction of two axisymmetric bodies falling side by side at moderate Reynolds numbers. *J. Fluid Mech.* **741**, R6.

ERN, P., RISSO, F., FABRE, D. & MAGNAUDET, J. 2012 Wake-induced oscillatory paths of freely rising or falling bodies. *Annu. Rev. Fluid Mech.* **44**, 97–121.

FERNANDES, P. C., ERN, P., RISSO, F. & MAGNAUDET, J. 2005 On the zigzag dynamics of freely moving axisymmetric bodies. *Phys. Fluids* **17** (9), 098107.

FERNANDES, P. C., ERN, P., RISSO, F. & MAGNAUDET, J. 2008 Dynamics of axisymmetric bodies rising along a zigzag path. *J. Fluid Mech.* **606**, 209–223.

FERNANDES, P. C., RISSO, F., ERN, P. & MAGNAUDET, J. 2007 Oscillatory motion and wake instability of freely rising axisymmetric bodies. *J. Fluid Mech.* **573**, 479–502.

FORTES, A. F., JOSEPH, D. D. & LUNDGREN, T. S. 1987 Nonlinear mechanics of fluidization of beds of spherical particles. *J. Fluid Mech.* **177**, 467–483.

HALLEZ, Y. & LEGENDRE, D. 2011 Interaction between two spherical bubbles rising in a viscous liquid. *J. Fluid Mech.* **673**, 406–431.

HU, H. H., JOSEPH, D. D. & CROCHET, M. J. 1992 Direct simulation of fluid particle motions. *Theor. Comput. Fluid Dyn.* **3**, 285–306.

JAYAWEERA, K. O. L. F. & MASON, B. J. 1965 The behaviour of freely falling cylinders and cones in a viscous fluid. *J. Fluid Mech.* **33**, 709–720.

JAYAWEERA, K. O. L. F., MASON, B. J. & SLACK, G. W. 1964 The behaviour of clusters of spheres falling in a viscous fluid. Part 1. Experiment. *J. Fluid Mech.* **20** (1), 121–128.

JOHNSON, T. A. & PATEL, V. C. 1999 Flow past a sphere up to a Reynolds number of 300. *J. Fluid Mech.* **378**, 19–70.

KOK, J. B. W. 1993*a* Dynamics of pair of gas bubbles moving through liquid. Part 1: theory. *Eur. J. Mech.* B/*Fluids* **12**, 515–540.

KOK, J. B. W. 1993*b* Dynamics of pair of gas bubbles moving through liquid. Part 2: experiment. *Eur. J. Mech.* B/*Fluids* **12**, 541–560.

LEGENDRE, D. & MAGNAUDET, J. 1998 The lift force on a spherical bubble in a viscous linear shear flow. *J. Fluid Mech.* **368**, 81–126.

MAGNAUDET, J. 1997 The forces acting on bubbles and rigid particles. In *ASME Fluids Engng Division Summer Meeting (FEDSM'97)*, pp. 1–9.

MAGNAUDET, J. & EAMES, I. 2000 The motion of high-Reynolds-number bubbles in inhomogeneous flows. *Annu. Rev. Fluid Mech.* **32**, 659–708.

MENEGHINI, J. R., SALTARA, F., SIQUEIRA, C. L. R. & FERRARI, J. A. 2001 Numerical simulation of flow interferance between two circular cylinders in tandem and side-by-side arrangements. *J. Fluids Struct.* **15** (2), 327–350.

MITTAL, S., KUMAR, V. & RAGHUVANSHI, A. 1997 Unsteady incompressible flows past two cylinders in tandem and staggered arrangements. *Intl J. Numer. Meth. Fluids* **25** (11), 1315–1344.

MIZUSHIMA, J. & NORIHISA, S. 2005 Instability and transition of flow past two tandem circular cylinders. *Phys. Fluids* **17** (10), 104107.

MOORE, D. W. 1963 The boundary layer on a spherical gas bubble. *J. Fluid Mech.* **16** (2), 161–176.

NATARAJAN, R. & ACRIVOS, A. 1993 The instability of the steady flow past spheres and disks. *J. Fluid Mech.* **254**, 323–344.

TSUJI, Y., MORIKAWA, Y. & TERASHIMA, Y. 1982 Fluid-dynamic interaction between two spheres. *Intl J. Multiphase Flow* **8** (1), 71–82.

TSUJI, T., NARUTOMI, R., YOKOMINE, T., EBARA, S. & SHIMIZU, A. 2003 Unsteady three-dimensional simulation of interactions between flow and two particles. *Intl J. Multiphase Flow* **29** (9), 1431–1450.

YUAN, H. & PROSPERETTI, A. 1994 On the in-line motion of two spherical bubbles in a viscous fluid. *J. Fluid Mech.* **278**, 325–349.

ZHU, C., LIANG, S. C. & FAN, L. S. 1994 Particle wake effects on the drag force of an interactive particle. *Intl J. Multiphase Flow* **20** (1), 117–129.